Synthesis and Gas Permeation Properties of Tetraoxidethianthrene-Based Polymers of Intrinsic Microporosity

Received 00th January 20xx,
Accepted 00th January 20xx

DOI: 10.1039/x0xx00000x

Sarah A. Felemban,[a] C. Grazia Bezzu,[b] Bibiana Comesaña-Gándara,[a] Johannes C. Jansen,*[,c] Alessio Fuoco,[c] Elisa Esposito,[c] Mariolino Carta*[,d] and Neil B. McKeown*[,a]

A series of nine polymers of intrinsic microporosity (PIMs) derived from different bis-catechol monomers and 2,3,7,8-tetrafluoro-5,5',10,10'-tetraoxidethianthrene (TOT) were synthesised and tested for their potential use as gas separation membranes. As powders, they demonstrate significant nitrogen adsorption at 77 K allowing apparent BET surface areas ranging from 432-785 $m^2 g^{-1}$ to be calculated. Six of the polymers were found to be soluble in quinoline facilitating the casting of self-standing films to allow the assessment of their gas separation properties. Spirobifluorene-based polymers exhibited the highest gas permeability, approaching the performance of the archetypal PIM-1, and the data for some are placed close to the 2008 Robeson upper bounds for O_2/N_2 and CO_2/CH_4. Ageing studies showed a gradual decrease in permeability, accompanied by an increase in selectivity that moved the data more-or-less parallel to the Robeson upper bounds. The two polymers with the lowest and highest gas permeability were both tested over the temperature range 25-55°C and an enhancement in permeability for all gases, with exception of CO_2, was observed along with decreased selectivity for almost all gas pairs. The latter seems to be due to the simultaneous drop in both diffusivity selectivity and solubility selectivity for all gas pairs, but especially those involving CO_2, due to a strong decrease in solubility with increasing temperature. The analysis of the energetic and entropic selectivity provides further insight into the remarkable transport properties of PIMs. Overall, the tetraoxidethianthrene unit proves to be a suitable building block for use in PIM synthesis for applications in gas separation membranes and these PIMs have a one to two orders of magnitude higher permeability than more common polysulfones.

Introduction

Microporous organic polymeric materials[1] have been at the centre of increasing interest over the past few decades due to their potential applications in catalysis,[2] gas separation membranes,[3] gas storage[4, 5] and as adsorbents for organic compounds.[6-8] In 2004, a significant advance in this field was reported with the preparation of novel porous polymers, named Polymers of Intrinsic Microporosity (PIMs), derived from purely organic monomers and processable from solution into robust films and coatings. PIMs possess highly rigid and contorted structures, which generate microporosity by restricting the conformational flexibility and preventing efficient packing of the polymeric chains. The archetypal[9] PIM-1 was prepared *via* the double nucleophilic aromatic substitution between 5,5',6,6'-tetrahydroxy-3,3,3',3'-tetramethylspirobisindane (TTSBI) and 2,3,5,6-tetrafluoro-terephthalonitrile (TFTPN) (Scheme 1). In addition to microporosity, demonstrated by nitrogen adsorption, and high molecular mass, it is fully soluble in common organic solvents such as chloroform and tetrahydrofuran and can be cast from solution into self-standing films. PIM-1 exhibits high gas permeability and good selectivity for some important commercial gas pairs, such as O_2/N_2, CO_2/CH_4, H_2/N_2, with overall performance that helped to define many of the 2008 Robeson upper bounds.[10]

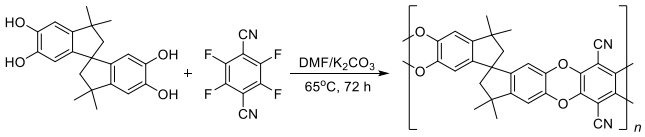

Scheme 1. The synthesis of PIM-1

Subsequently, numerous other soluble PIMs with similar or enhanced properties for gas separation have been successfully synthesised. An attractive idea is to include sulphur-based components such as trifluoromethylphenylsulfone which was first reported by Guiver's group.[11] The resulting ladder PIMs (e.g. TFMPS-PIM) showed intrinsic microporosity, high molecular weight (M_n > 55000) and good performance for gas separations. Compared to PIM-1, they exhibited higher selectivity, coupled with a decreased permeability, for gas pairs such as O_2/N_2 and CO_2/N_2, with increasing content of trifluoromethylphenylsulfone.[12] Subsequently, Guiver's group reported the synthesis of co-polymers that included another sulfone containing monomer, 2,3,7,8-tetrafluoro-5,5',10,10'-tetraoxidethianthrene (**TOT**), all of which exhibited apparent BET surface areas between 408-709 $m^2 g^{-1}$ calculated from N_2 adsorption, and good film-forming properties. These polymers again showed a decrease in permeability, combined with a corresponding increase in selectivity, for gas pairs such as O_2/N_2, CO_2/N_2 and H_2/N_2 when compared to PIM-1.[13] Inspired

[a] *EaStCHEM, School of Chemistry, University of Edinburgh, Joseph Black Building, David Brewster Road, Edinburgh, Scotland EH9 3FJ, UK;*
[b] *School of Chemistry, Cardiff University, Cardiff CF10 3AT, U.K.*
[c] *Institute on Membrane Technology, CNR-ITM, Via P. Bucci 17/C, 87036 Rende (CS), Italy*
[d] *Department of Chemistry, College of Science, Swansea University, Grove Building, Singleton Park, Swansea, SA2 8PP, UK.*
Electronic Supplementary Information (ESI) available: [details of any supplementary information available should be included here]. See DOI: 10.1039/x0xx00000x

by this work, and by a theoretical study that predicted enhanced solubility selectivity for PIMs containing the sulfonyl group for separations involving CO_2,[14] we aimed to expand the structural diversity of sulfonyl-containing PIMs.

We targeted the reaction of the **TOT** monomer with different bis-catechols (Figure 1), which contain attractive and characteristic structural features that had previously been used to prepare high performing PIMs as membranes for gas separation. The initial TOT-based polymer reported by Guiver's group[13] (here denoted as **PIM-TOT-100**) was also reproduced by reacting (TTSBI) **1** with **TOT** to allow a direct comparison between gas permeability results. We also extended the series with the combination of **TOT** with other bis-catechol monomers, such as spirobichroman **2**,[15] 9,9-bis(3,4-dihydroxyphenyl) fluorene **3**, which contains a cyclic unit that forms a "cardo-polymer".[16] Importantly, we selected spirobifluorene (SBF) bis-catechols (2,2',3,3'-tetrahydroxy-9,9'-spirobifluorene **4a**, 2,2',3,3'-tetrahydroxy-6,6'-*dimethyl*-9,9'-spirobifluorene **4b**, and 2,2',3,3'-tetrahydroxy-6,6'-*t-butyl*-9,9'-spirobifluorene **4c**) previously used to prepare PIMs with excellent performance.[17] In addition, tetrahydroxy ethanoanthracene **5**,[18] which contains a bridged bicyclic ring system, similar to the one that was successfully used to make a new category of PIMs based on Tröger's base,[19] and tetrahydroxyhexaphenylbenzene (HPB)[20] **6**, which consists of six benzene rings connected to a single central benzene ring, were also chosen. Finally, we used the triptycene containing bis-catechol **7**, which lead to an unusual 2D chain packing when polymerized with TFTPN, translating into a significant improvement of the CO_2 permeability.[21, 22] Unfortunately, the **TOT** polymers obtained from monomers **5**, **6** and **7** did not form films because of their insolubility in common organic solvents (Table 1).

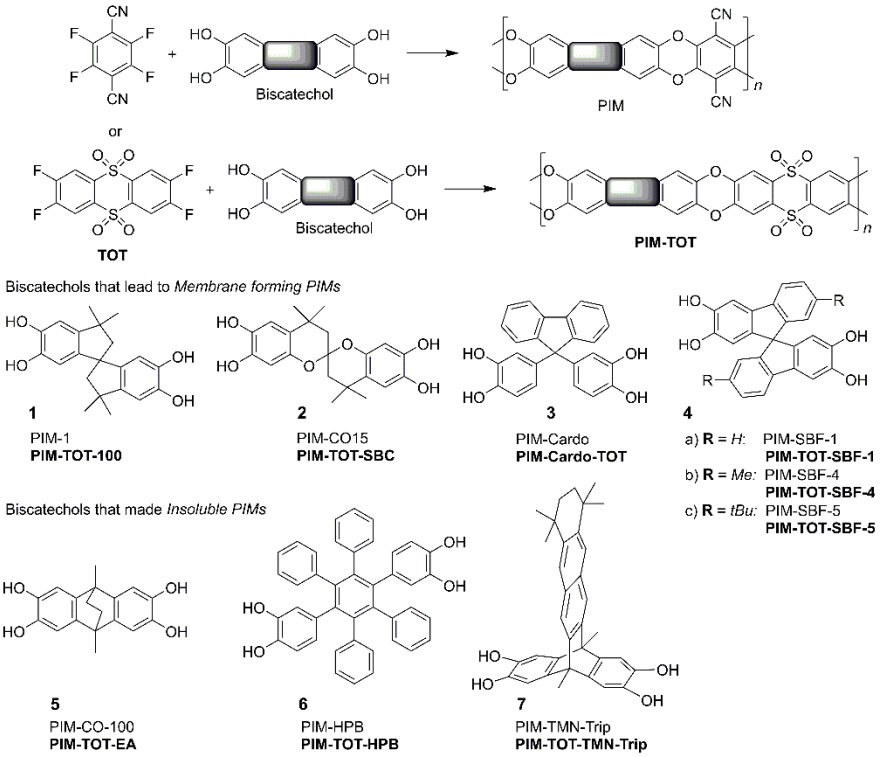

Figure 1. Monomers for PIM-TOT (in bold) and related names for previously published PIMs prepared from the same bis-catechols and tetrafluoroterephthalonitrile (TFTPN).

Experimental part

General methods and equipment

Commercially available reagents were used without further purification. Anhydrous *N,N*-dimethylformamide was bought from Sigma-Aldrich. All reactions using air/moisture sensitive reagents were performed in oven-dried apparatus, under a nitrogen atmosphere. Low-temperature (77 K) N_2 and CO_2 (273 K) adsorption/desorption measurements of PIM powders were made using a Quantachrom Quadrasorb Evo. Samples were degassed for 800 min at 120 °C under high vacuum prior to analysis. The data were analysed with the software provided with the instrument. Non-local density functional theory (NLDFT) and Horvath–Kawazoe (H-K) analysis was performed to calculate the pore size distribution and volume, considering a carbon equilibrium transition kernel at 273 K based on a slit-pore model; the kernel is based on a common, one centre, Lennard-Jones model. Solid state ^{13}C NMR spectra were obtained using a 400 MHz HFXY Bruker Avance III spectrometer at St Andrews University. Infrared adsorption spectra of powder samples were recorded on a Shimadzu IR Affinity-1S FTIR spectrophotometer. TGAs were performed using the device Thermal Analysis SDT Q600 at a heating rate of 10 °C min^{-1} from room temperature to 1000 °C in N_2 atmosphere.

Monomer and polymer synthesis

Monomers 1 and 2 came from commercial sources (**1** Sigma-Aldrich, 96%, **2** Alfa-Aesar 97% both recrystallized from DCM).

Monomers **3**,[23] **4 (a-c),**[17] **5,**[17] **6**[20] and **7**[21] were synthesised according to published procedures. Intermediate steps and details of the synthesis of **TOT** are given in the ESI.

General procedure for polymer synthesis

According to a reported procedure,[24] 2,3,7,8-tetrafluoro-5,5',10,10'-tetraoxide-thianthrene (1 equivalent) and bis-catechol monomer (1 equivalent) were dissolved in N-methyl-2-pyrrolidone. To this, an excess of potassium carbonate was added and the reaction mixture was stirred under a nitrogen atmosphere at the desired temperature as in Scheme 1 but with **TOT** instead of TFTPN. Then, the reaction mixture was poured into water. The precipitate was collected by filtration, refluxed in water, acetone and methanol, and dried in the vacuum oven at 100 °C. Details of the individual polymers are given in the ESI. As a typical example, the synthesis of **PIM-TOT-SBC** is described below; those of the other polymers are reported in the ESI. In addition, **PIM-Cardo** was re-synthesised according to a patent procedure[25] as its gas permeability data have never been previously reported due to a perceived lack of solubility for processing.[12]

2,3,7,8-Tetrafluoro-5,5',10,10'-tetraoxidethianthrene (**TOT**) (0.500 g, 1.419 mmol), 6,6',7,7'-tetrahydroxy-4,4,4',4'-tetramethyl-2,2'-spirobichroman **2** (0.528 g, 1.419 mmol), *N*-methyl-2-pyrrolidone (20 mL) and potassium carbonate (3.14 g, 22.7 mmol) were reacted at 70 °C for 72 hours to give a pale yellow powder (0.74 g, 1.15 mmol, 81%) which was soluble in quinoline; ν_{max} (cm^{-1}) 2925, 1590, 1471, 1427, 1328, 1292, 1242, 1132, 908, 875, 719; ^{13}C NMR (solid state; 101 MHz) δ 146.6, 136.2, 129.3, 113.7, 105.8, 98.5, 46.5, 31.3; BET surface area = 471 $m^2\ g^{-1}$; Total pore volume (calculated at P/P_0 = 0. 9793) = 0.3532 $cm^3\ g^{-1}$. TGA (nitrogen): weight loss due to thermal degradation started at 415 °C.

Gas permeation measurements

Film samples were 6 cm in diameter with a thickness in the range of 150-200 micrometres. An effective area of 2.14 cm^2 inside the footprint of the sealing ring was used for analysis. Gas permeability measurements were performed on a constant-volume/variable-pressure instrument constructed by EESR (Geesthacht, Germany) following the design of HZG (Geesthacht). The membrane samples, typically with an exposed area of 2.14 cm^2, were completely degassed under vacuum for at least 30 minutes before the measurements until all absorbed species were removed, and measurements were then carried out with the following gases: He, H_2, O_2, N_2, CH_4 and CO_2 (purity of 99.99+%, SAPIO, Italy). All membranes were stored in air at ambient conditions during the aging process and evacuated long enough to remove traces of humidity that might have absorbed from the air before the measurement. Details on the instrument and procedures can be found elsewhere.[26] The permeability coefficient, *P*, of the membrane with thickness, *l*, and area, *A*, is calculated from the increase in the permeate pressure, p_t, as a function of time, *t*, in pseudo-steady state at absolute temperature, *T*, for a given feed pressure, p_f:

$$p_t = p_0 + (dp/dt)_0 \cdot t + \frac{RT \cdot A}{V_P \cdot V_m} \cdot \frac{p_f \cdot P}{l}\left(t - \frac{l^2}{6D}\right) \qquad \text{Eq. 1}$$

where *R* is the universal gas constant, V_P the permeate volume and V_m the molar gas volume at STP conditions. The initial pressure p_0 and the leak flow rate $(dp/dt)_0$ are normally negligible but can be corrected for, if needed. The diffusion coefficient, *D*, is calculated from the so-called permeation time lag[27], Θ:

$$\Theta = \frac{l^2}{6D} \qquad \text{Eq. 2}$$

The time lag can be obtained from the intersection of the tangent to the pseudo-steady-state pressure-increase curve and the time axis. Assuming the solution-diffusion mechanism, the gas solubility coefficient, *S*, is obtained indirectly from the ratio of the permeability and the diffusion coefficient:

$$S = P/D \qquad \text{Eq. 3}$$

Results and discussion

Synthesis of 2,3,7,8-tetrafluoro-5,5',10,10'-tetraoxidethianthrene (TOT)

The key monomer **TOT** (Figure 1) was synthesised by modifying the procedure originally reported by Du *et al*.[13] to make the thianthrene intermediate which, in our hands, gave very poor yields (<3%). Firstly, room temperature was found to be optimal and, secondly, after screening several different solvents, nitromethane proved more effective than chloroform. As a result of these simple modifications, the overall yield of tetrafluorothianthrene was increased significantly. Moreover, a purer product was obtained after a simple recrystallization using chloroform, which prevented the need for purification by column chromatography. The detailed synthesis of the precursor and monomer is reported in the ESI.

Synthesis of bis-catechols (1-7)

Among the series of selected bis-catechols, the spirobisindane (TTSBI) **1** and the spirobichroman (SBC) **2** are commercially available and were used after a quick recrystallization from ethanol. This affords purer compounds that lead to an improvement in the degree of polymerisation and allows the formation of more robust films. The synthesis of fluorene **3**, that leads to the polymers **PIM-Cardo** and **PIM-Cardo-TOT**, was achieved following a patent procedure.[23] The spirobifluorenes (SBFs, **4a-c**), where **4a** represents the unsubstituted SBF, **4b** the SBF with methyl groups in positions 6 and 6' and **4c**, with t-butyl groups in the same positions, were synthesised according to the procedures reported in our previous work.[17] The tetrahydroxyanthracene bis-catechol **5** was synthesised according to the method reported by Niederl and Nagel.[28] The hexaphenylbenzene monomer **6**[20] and, finally, the triptycene based monomer **7**[21] were prepared according to previously reported procedures.

Synthesis and characterization of polymers

A series of polymers, namely **PIM-TOT-100**, **PIM-TOT-SBC**, **PIM-Cardo-TOT**, **PIM-TOT-SBF-1**, **PIM-TOT-SBF-4**, **PIM-TOT-SBF-5**, **PIM-TOT-EA**, **PIM-TOT-HPB** and **PIM-TOT-TMN-Trip**, derived from combination of **TOT** with bis-catechol-based monomers **1-7** was synthesised, according to a general procedure used for PIMs synthesis.[24] This involved reacting the two monomers in NMP in the presence of K_2CO_3 at 70 °C for 72 hours, *via* the typical double nucleophilic aromatic substitution that provides the dioxin linking group. The polymers all demonstrated poor solubility in common deuterated solvents preventing characterisation by solution NMR. Therefore, they were characterized by solid-state ^{13}C NMR, FTIR, thermogravimetric analysis (TGA) and BET surface area measurements. Details of the physical properties of each polymer are provided in Table 1 and in the ESI. In addition, the physical data for the polymers derived from the same bis-catechols but with the archetypal TFTPN as the fluorinated monomer, are also provided in the same table for comparison.

Physical properties of TOT-polymers

The infrared spectrum for each polymer sample in powder form confirmed the presence of two characteristic sulfonyl peaks in the range of (1400 – 1100) cm^{-1}. In addition, the absence of the OH stretch (3400- 2700 cm^{-1}), provides good evidence that the reaction of the bis-catechols with 2,3,7,8-tetrafluoro-5,5',10,10'-tetraoxidethianthrene **TOT** was efficient. The thermal properties of the polymers, evaluated by TGA under N_2 flow, demonstrated excellent thermal stability with decomposition temperatures above 400 °C, apart from **PIM-TOT-EA**, which shows the typical mass reduction associated with the loss of the ethylene bridge *via* retro-Diels-Alder reaction at ~300 °C (Figure ESI2 and ESI3). The polymers in powder form demonstrated high intrinsic microporosity, with large amounts of N_2 adsorbed, at low pressure, at 77 K and CO_2 at 273 K (Figure 2). Apparent BET surface areas of the powder samples were calculated (Table 1) with all TOT-derived polymers demonstrating values ranging from 432 to 785 $m^2\ g^{-1}$. The data clearly show that the surface areas of the polymers with well-defined sites of contortion, such as those obtained from SBF or TMN-Trip monomers, provided larger BET as compared to those with SBC, Cardo or the HPB units, which possess greater rotational freedom and flexibility. In general, all **TOT**-derived polymers showed slightly lower surface areas compared to the related PIMs prepared from the same bis-catechol monomers and TFTPN (Table 1). This trend could be explained by the larger size of the TOT unit as compared to TFTPN (Figure 1), leading to an effective decrease in the concentration of sites of contortion along the polymer chain, which may result in a more efficient packing of the polymer. The evaluation of the total pore volume, indicates that the SBF containing polymers have the highest amount of free volume, with **PIM-TOT-SBF-5** showing the highest values, which is consistent with results from PIM-SBFs based on TFTPN.[17] In accordance with the highest BET values, as measured with N_2, **PIM-TOT-TMN-Trip** showed also the highest CO_2 uptake, followed by that of the SBFs series (Figure 2B and Table 1). The pore size distribution (PSD, Figure ESI2), measured from the CO_2 uptake at 273 K and evaluated by the NLDFT and H-K models considering the adsorbent geometry as carbon slit pores for all cases,[29] confirmed the microporous nature of these PIMs and indicates that **PIM-TOT-TMN-Trip** has the greatest relative contribution of ultramicropores, followed by members of the SBFs series and with **PIM-TOT-HPB** and **PIM-TOT-SBC** having the lowest contribution.

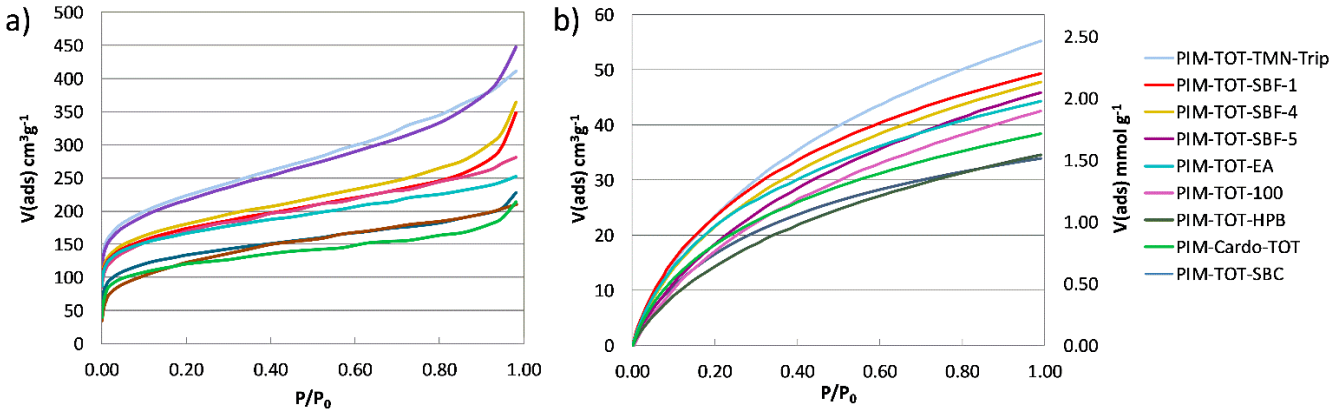

Figure 2. Isotherms of PIM-TOTs a) from N_2 adsorption at 77 K (desorption curves were removed for clarity); b) from CO_2 adsorption at 273 K.

Table 1 Physical characterization of TOT – derived polymers in comparison with the corresponding TFTPN-based polymers.

Monomers	Polymer	Solubility	S_{BET} from N_2 adsorption, $m^2\ g^{-1}$	Pore Volume, $cm^3\ g^{-1}$	T_d, °C	CO_2 uptake @ 273 K, mg g^{-1} (mmol g^{-1})
1 + TOT	PIM-TOT-100	Yes [a]	596	0.44	430	43 (1.9)
	(PIM-TOT-100[13]) [b]	Yes	560	-	472	-
2 + TOT	PIM-TOT-SBC	Yes [a]	471	0.35	415	34 (1.5)
3 + TOT	PIM-Cardo-TOT	Yes [a]	432	0.33	440	39 (1.7)
4a + TOT	PIM-TOT-SBF-1	Yes [a]	611	0.54	424	49 (2.2)
4b + TOT	PIM-TOT-SBF-4	Yes [a]	637	0.57	439	48 (2.1)
4c + TOT	PIM-TOT-SBF-5	Yes [a]	762	0.69	450	46 (2.1)
5 + TOT	PIM-TOT-EA	No	601	0.39	405	44 (2.0)
6 + TOT	PIM-TOT-HPB	No	433	0.33	431	35 (1.6)
7 + TOT	PIM-TOT-TMN-Trip	No	785	0.64	425	56 (2.5)
1 + TFTPN	PIM-1[9]	Yes	760	0.78	370	-
2 + TFTPN	PIM-CO15[15]	Yes	510	0.38	390	-
3 + TFTPN	PIM-Cardo This work	Yes [a]	384	0.27	541	40 (1.8)
4a + TFTPN	PIM-SBF-1[17]	Yes	803	0.74	565	54 (2.4)
4b + TFTPN	PIM-SBF-4[17]	Yes	752	0.59	530	63 (2.8)
4c+ TFTPN	PIM-SBF-5[17]	Yes	882	0.73	490	56 (2.5)
5+ TFTPN	PIM-CO-100[18]	No	630	-	-	-
6+ TFTPN	PIM-HPB[20]	Yes	537	0.65	515	-
7+ TFTPN	PIM-TMN-Trip[21]	Yes	1050	0.87	474	74 (3.3)

[a] Only quinoline yields mechanically stable membranes suitable for gas separation. **Other solvent tested were, $CHCl_3$, dichloroethane, chlorobenzene, THF, as well as the polar aprotic solvents DMAc and NMP. All solubility tests were conducted at room temperature.** [b] Data from Du et al. for comparison[13]

Membrane formation and gas permeation properties

Films were formed from **PIM-TOT-100**, **PIM-TOT-SBC**, **PIM-Cardo-TOT**, **PIM-TOT-SBF-1**, **PIM-TOT-SBF-4**, and **PIM-TOT-SBF-5** by the slow evaporation (over two weeks) of a solution of each polymer in quinoline. Despite high boiling point of quinoline (237 °C), which is not ideal for rapid film formation, it proved a suitable solvent.

Table 2 Gas permeabilities P_a, and ideal selectivities α for methanol treated films TOT-PIMs. Data from aged films (between 114 and 1028 days) in brackets. PIM-Cardo, PIM-1, PIM-SBF-1, PIM-SBF-4 and PIM-SBF-5 are reported for comparison. (1 Barrer = 10^{-10} cm^3(STP) cm cm^{-2} s^{-1} $cmHg^{-1}$)

Polymer	P_a [Barrer]						Ideal selectivity α (P_a/P_b)			
	N_2	O_2	CO_2	CH_4	H_2	He	H_2/N_2	CO_2/N_2	O_2/N_2	CO_2/CH_4
PIM- TOT-100	281	943	5670	465	2380	934	8.5	20.2	3.4	12.2
(680 days)	(105)	(401)	(2360)	(140)	(1360)	(623)	(12.9)	(22.4)	(3.8)	(16.8)
PIM-TOT-SBC	43.7	181	1100	57.8	742	370	16.9	25.0	4.1	19.1
(1028 days)	(18.1)	(79)	(471)	(21.2)	(400)	(240)	(221)	(26.0)	(4.3)	(22.2)
PIM-Cardo-TOT	46.0	186	1026	52.3	730	329	15.9	22.3	4.0	19.6
(885 days)	(23.9)	(104)	(651)	(25.5)	(508)	(254)	(21.3)	(27.3)	(4.4)	(25.5)
PIM-TOT-SBF-1	284	938	5435	392	2380	874	8.4	19.1	3.3	13.9
(807 days)	(79)	(303)	(1820)	(102)	(1090)	(465)	(13.8)	(23.0)	(3.3)	(17.8)
PIM-TOT-SBF-4	362	1200	6740	500	3130	1110	8.6	18.6	3.3	13.5
(738 days)	(145)	(544)	(3060)	(184)	(1770)	(679)	(12.2)	(21.1)	(3.8)	(16.6)
PIM-TOT-SBF-5	717	1960	11400	1430	4160	1520	5.8	15.9	2.7	8.0
(543 days)	(322)	(1008)	(5715)	(570)	(2567)	(1007)	(8.0)	(17.7)	(3.1)	(10.0)
PIM-1[30]	857	2200	13300	1150	4500	1706	5.3	15.5	2.6	11.6
(1200 days)	(125)	(600)	(2840)	(159)	(2400)	(1140)	(19.2)	(22.7)	(4.8)	(17.9)
PIM-Cardo This work	135	490	3110	187	1520	615	11.2	23.0	3.63	16.6
(114 days)	(57.6)	(239)	(1470)	(71.5)	(934)	(426)	(16.2)	(25.5)	(4.15)	(20.5)
PIM-SBF-1[17]	340	1420	8850	532	4330	1560	12.7	26.0	4.2	16.6
(2088 days)	(87.5)	(486)	(2410)	(102)	(2190)	(914)	(25.0)	(27.5)	(5.6)	(23.6)
PIM-SBF-4[17]	474	1760	10600	834	4900	1930	10.3	22.4	3.7	12.7
(1428)	(286)	(1260)	(6410)	(331)	(3960)	(1470)	(13.8)	(22.4)	(4.4)	(19.4)
PIM-SBF-5[17]	1080	2750	16400	2480	5590	2060	5.2	15.2	2.5	6.6
(1439)	(550)	(1870)	(10000)	(925)	(4710)	(1830)	(8.6)	(18.2)	(3.4)	10.8

Also, **PIM-Cardo**, for which it had previously been impossible to obtain a stable film from low-boiling solvents,[12] formed a good membrane in quinoline. High quality film formation was achieved using a levelled heating system set at 60 °C to aid the slow evaporation of quinoline. Subsequently, the films were washed several times with methanol to remove the quinoline and then dried in a vacuum oven at 120 °C. The complete removal of the residual solvent was confirmed by thermogravimetric analysis (TGA, Figure ESI3, Figure ESI4). The formation of robust self-standing films confirmed that the molecular mass of each of these polymers was high showing the efficiency of the reaction of the bis-catechols with **TOT**. This is an important conclusion in the absence of a direct molecular mass measurement using gel permeation chromatography (GPC).

Gas permeability, P_x, measurements using these films were performed using time lag and steady state permeation measurements and were used to calculate ideal selectivities (P_x/P_y) (Table 2). The diffusion and solubility coefficients derived from the time-lag measurements are listed in Table ESI1 - Table ESI7. All polymers showed good performance, with data approaching or even exceeding the 2008 Robeson upper bounds, for some commercially important gas pairs, although remaining somewhat below the recently proposed upper bounds[22,31] (Figure 3). After the MeOH treatment, the three **SBF**-based TOT-PIMs showed the highest permeabilities, with that based on the *t-butyl* substitution (**PIM-TOT-SBF-5**) being the most permeable of the series, in accordance with the trends noted for the PIM-SBF series but at lower permeability.[17]

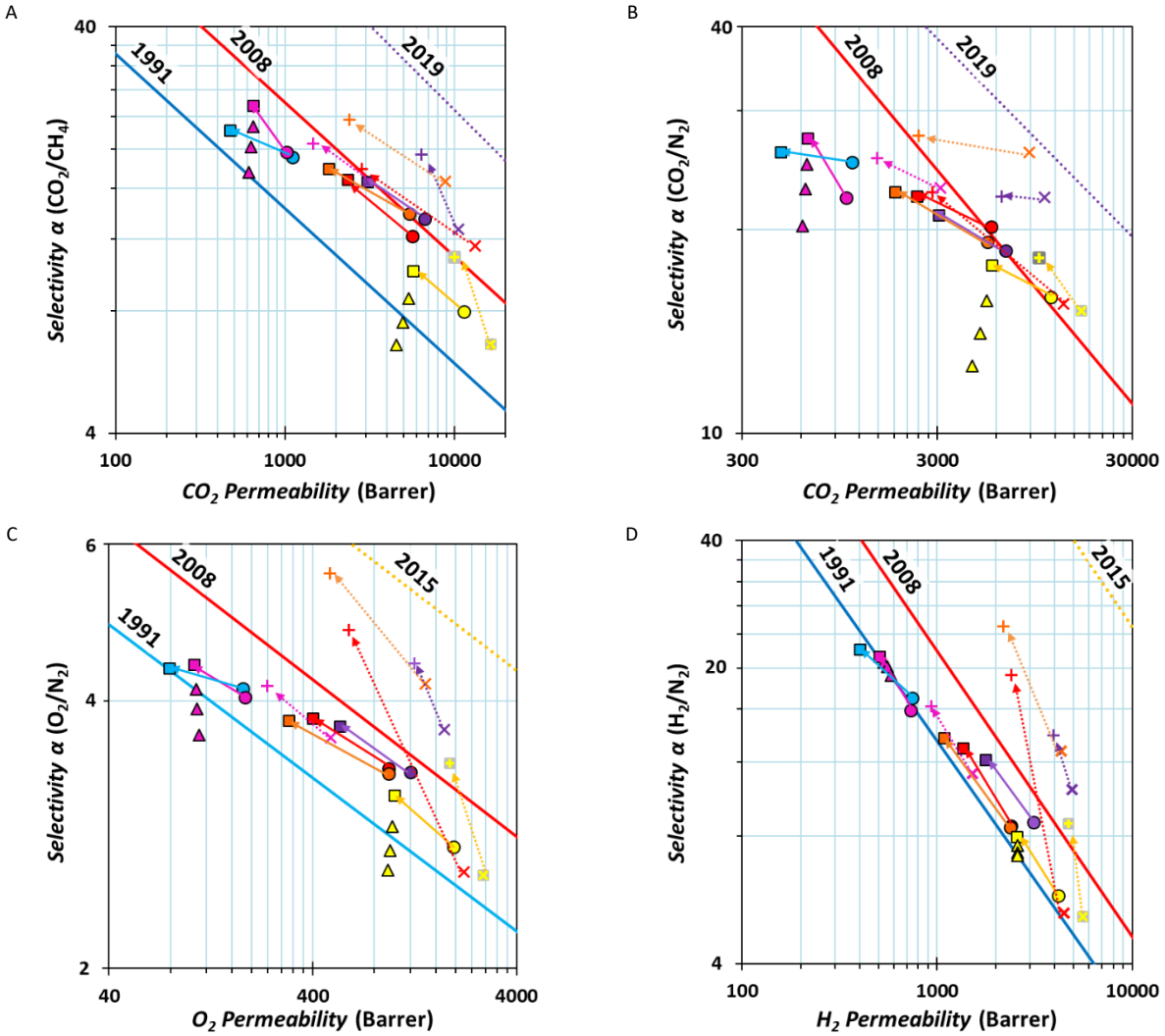

Figure 3. Robeson plots for the (A) CO_2/CH_4, (B) CO_2/N_2, (C) O_2/N_2, and (D) H_2/N_2 gas pairs showing the position of the gas permeability data for films of TOT-PIM-100 (●,■), PIM-TOT-SBC (●,■), PIM-TOT-SBF-1 (●,■), PIM-TOT-SBF-4 (●,■), PIM-TOT-SBF-5 (○,□), PIM-Cardo-TOT (●,■). All data measured at 25°C unless stated otherwise, and MeOH treated samples indicated as circles (○) and samples in the age range 543-1028 days indicated as squares (□). Temperature-dependent measurements performed on the aged samples of PIM-TOT-SBF-5 and PIM-Cardo-TOT at 35°C, 45°C and 55°C are reported as triangles (△,▲) with the same colour as the corresponding samples tested at 25°C (□,■). The equivalent TFTPN-PIMs are shown for comparison in the same colours as the TOT-PIMs with symbols "x" (fresh) and "+" (aged): PIM-1 (x,+),[30] PIM-SBF-1 (x,+),[17] PIM-SBF-4 (x,+),[17] PIM-SBF-5 (x,+),[17] and PIM-Cardo (x,+)[This work]. Upper bounds are represented by blue lines (Robeson 1991)[10], red lines (Robeson 2008)[12], yellow dotted lines for O_2/N_2 and H_2/N_2 (Swaidan 2015)[31], and purple dotted lines for CO_2/N_2 and CO_2/CH_4 (Comesaña-Gándara 2019)[22]. 1 Barrer = 10^{-10} cm^3(STP) cm cm^{-2} s^{-1} $cmHg^{-1}$.

The other two polymers in the SBF series, **PIM-TOT-SBF-4** and **PIM-TOT-SBF-1**, exhibit almost the same selectivity, coupled with a slightly higher permeability for **PIM-TOT-SBF-4** over **PIM-TOT-SBF-1**. The order of gas selectivities of the SBF family for the CO_2/CH_4, CO_2/N_2 and O_2/N_2 gas pairs is **PIM-TOT-SBF-1** > **PIM-TOT-SBF-4** > **PIM-TOT-SBF-5**. This trend is in accordance with the permeability/selectivity trade-off. **PIM-Cardo-TOT** exhibits a surprisingly good performance, considering the low BET surface area compared to the other PIMs. It approaches the 2008 Robeson upper bounds for CO_2/N_2 and H_2/N_2 and exceeds the upper bound for O_2/N_2 gas pairs. In a direct performance comparison with PIM-1, **PIM-Cardo-TOT** shows lower permeability consistent with its lower microporosity but higher selectivities.Similar like-to-like comparison shows that, in general, the freshly MeOH treated PIMs containing TFTPN units have higher permeability with respect to their TOT-based equivalent, but the latter show higher selectivity. In comparison with simple polysulfones,[32] one of the classes of polymers that became successful as commercial gas separation membranes after their introduction under the name Prism[33] in the late 1970s, the TOT based ladder-like PIMs in this work show superior permeability and a similar (CO_2/N_2) or somewhat lower selectivity (CO_2/CH_4, O_2/N_2), with a performance much closer to the upper bounds (Figure ESI5). However, there was no clear evidence of the predicted enhancement of solubility selectivity due to the presence of the sulfone groups (Tables ESI1-6). This may be due to the greater cohesive interactions between sulfone groups on neighbouring chains preventing the predicted strong interactions with CO_2.[14]

Effect of physical aging and temperature

As commonly observed for PIMs,[34] the gas permeability decreases upon ageing, and in line with the permeability/selectivity trade-off, the selectivity increases accordingly, approximately parallel to the Robeson upper bounds (Figure 3). The samples were aged for a time varying from 543 to 1028 days. Since the largest change occurs in the first few months of aging,[30, 34, 35] all samples are believed to be roughly comparable, in spite of the absolute difference in age. In the series of polymers, the relative decrease in diffusion coefficient upon ageing is very similar for all gases (Figure ESI6, Table ESI1 - Table ESI7). This is shown in Figure 4 for the two extreme polymers, the most permeable **PIM-TOT-SBF-5** and the least permeable **PIM-Cardo-TOT**, and is relatable to previous observations in a series of ultrapermeable polymers,[22] where ageing led to a strong increase in size-selectivity of the polymers. The latter is ascribed to a tightening of the bottle-necks between free volume elements in these polymers, affecting the transport of large molecules more than that of small molecules.[36] The fact that the increase in selectivity of the TFTPN-PIMs is accompanied by a less drastic decrease in permeability with respect to the TOT-PIMs, suggests that bottle-necks are formed by a rearrangement of the FFV, without a strong reduction in the overall free volume of the polymers.
Measurements with increasing temperature in the range from 25 to 55 °C, even if with very different absolute values of permeability coefficients, showed similar trends in **PIM-TOT-SBF-5** and **PIM-Cardo-TOT**. Both showed a modest increase in permeability for H_2, He, N_2 and CH_4, a nearly constant permeability for O_2, and a decrease in the permeability of CO_2 (Figure 5A and Figure ESI8). One specific difference between these two polymers lies in the relative permeation rate of He with respect to O_2: He has a higher permeability than O_2 for

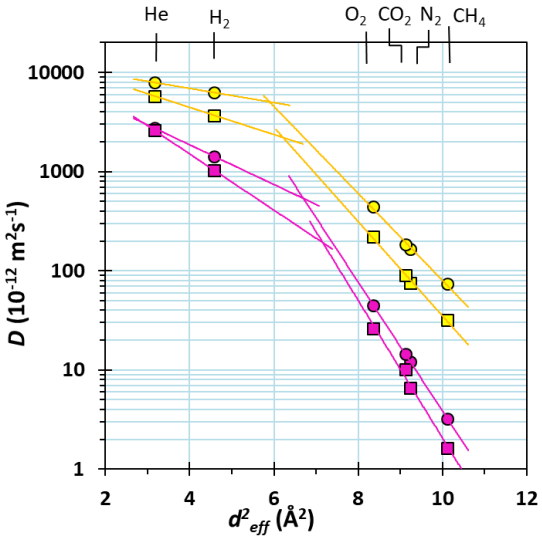

Figure 4. Plot of diffusivity coefficient, *D*, *versus* the squared effective diameter, d^2_{eff}, of the gas penetrant[37] for freshly methanol treated and aged films of PIM-TOT-SBF-5 (fresh ○, 543 days □) and Cardo-PIM-TOT (fresh ●, 885 days ■). Similar, analysis for the entire TOT-based PIMs family is reported in the supporting information Figure ESI6.

PIM-Cardo-TOT, while He and O_2 have a comparable permeability for **PIM-TOT-SBF-5** which is the typical behaviour for highly permeable PIMs.

The diffusivity in **PIM-TOT-SBF-5** is an order of magnitude higher than in **PIM-Cardo-TOT** for the bulkier gas CH_4, and for both PIMs it strongly increases with temperature (Figure 5B and Figure ESI9), while the diffusion selectivity decreases in a similar fashion in both polymers (Figure ESI7 and Figure ESI9). Both the solubility and the solubility selectivity decrease with increasing temperature, following similar trends for both polymers (Figure 5C and Figure ESI10). This effect dominates for CO_2, for which the strong decrease in permeability with increasing temperature is mostly due to the drop in the solubility of this highly soluble gas, which is not completely compensated by the increase in diffusivity (Figure ESI7). The trends in *P*, *D*, and *S* are all described by the typical Arrhenius behaviour and can be fitted with Eq. 4-Eq. 6.

$$P = P_0\, exp\left(\frac{-E_p}{RT}\right) \qquad \text{Eq. 4}$$

$$D = D_0\, exp\left(\frac{-E_d}{RT}\right) \qquad \text{Eq. 5}$$

$$S = S_0\, exp\left(\frac{-H_s}{RT}\right) \qquad \text{Eq. 6}$$

Where, R is the universal gas constant; T the absolute temperature; the pre-exponential factors P_0, D_0 and S_0 are the "y-intercepts" which are independent from the temperature, E_p is the activation energy of permeation, E_d is the activation

energy of diffusion, and H_s is the heat of sorption. The fitted values of E_p, E_d, and H_s for the **PIM-Cardo-TOT** and **PIM-TOT-SBF-5** are listed in Table 3. The values of E_p are positive for all gases, with the exception of CO_2 in both polymers and O_2 in **PIM-TOT-SBF-5**. This behaviour is uncommon for polymers traditionally used in gas separation membranes, but was also observed for ultrapermeable PTMSP[38] and PIM-TMN-Trip,[39] and is consistent with the decrease of permeability as a function of the temperature. All heats of sorption are negative and within the usual range for PIMs for H_2, He, O_2 and CO_2, while the heats of sorption for N_2 and CH_4 are remarkably high, among the highest values known for PIMs.[39,40] In general, the activation energies for diffusion are higher for **PIM-Cardo-TOT** than for **PIM-TOT-SBF-5** (Figure ESI11), but in both cases are close to that of the archetypal PIM-1.[40]

The diffusion selectivity is the expression of two different terms: the entropic selectivity, which is related to the change in the degree of freedom of a gas molecule that permeates through the material; and the energetic selectivity, which is related to the energy needed to open a motion-enabling-zone, (i.e. polymer chain rearrangement) for the activated gas diffusion. The analysis of these two terms has been performed for **PIM-TOT-SBF-5** and **PIM-Cardo-TOT** (Table 3), according to the transition theory of diffusion:[41]

$$\frac{D_a}{D_b} = \frac{\lambda_a^2}{\lambda_b^2} \underbrace{exp\left(\frac{\Delta S^*_{d(a,b)}}{R}\right)}_{entropic\ selectivity} \underbrace{exp\left(-\frac{\Delta E^*_{d(a,b)}}{RT}\right)}_{energetic\ selectivity} \qquad \text{Eq. 7}$$

where $\Delta S^*_{d(a,b)}$ is the difference in the activation entropy of diffusion for two gases (a and b); $\Delta E^*_{d(a,b)}$ is the difference in their activation energy of diffusion; and λ is the average diffusive jump, which is unknown, but its ratio λ_a^2/λ_b^2, can be approximated as d_a^2/d_b^2, where d is the effective diameter of the two gases taken into account.[42,27] The analysis of this contribution has been performed on the most permeable **PIM-TOT-SBF-5** and the least permeable **Cardo-PIM-TOT**. These two polymers demonstrate a low O_2/N_2 entropic selectivity (<1), which is related to the higher degree of freedom of O_2 with respect to N_2 in the micropores, which is then lost in the diffusion through a motion-enabled-zone. Their values are half-way between that of PIM-1 and Triptycene-based PIMs[39] and very close to the so-called "hyper-rigid" 6FDA-PMDA-TAB (10:90).[43]

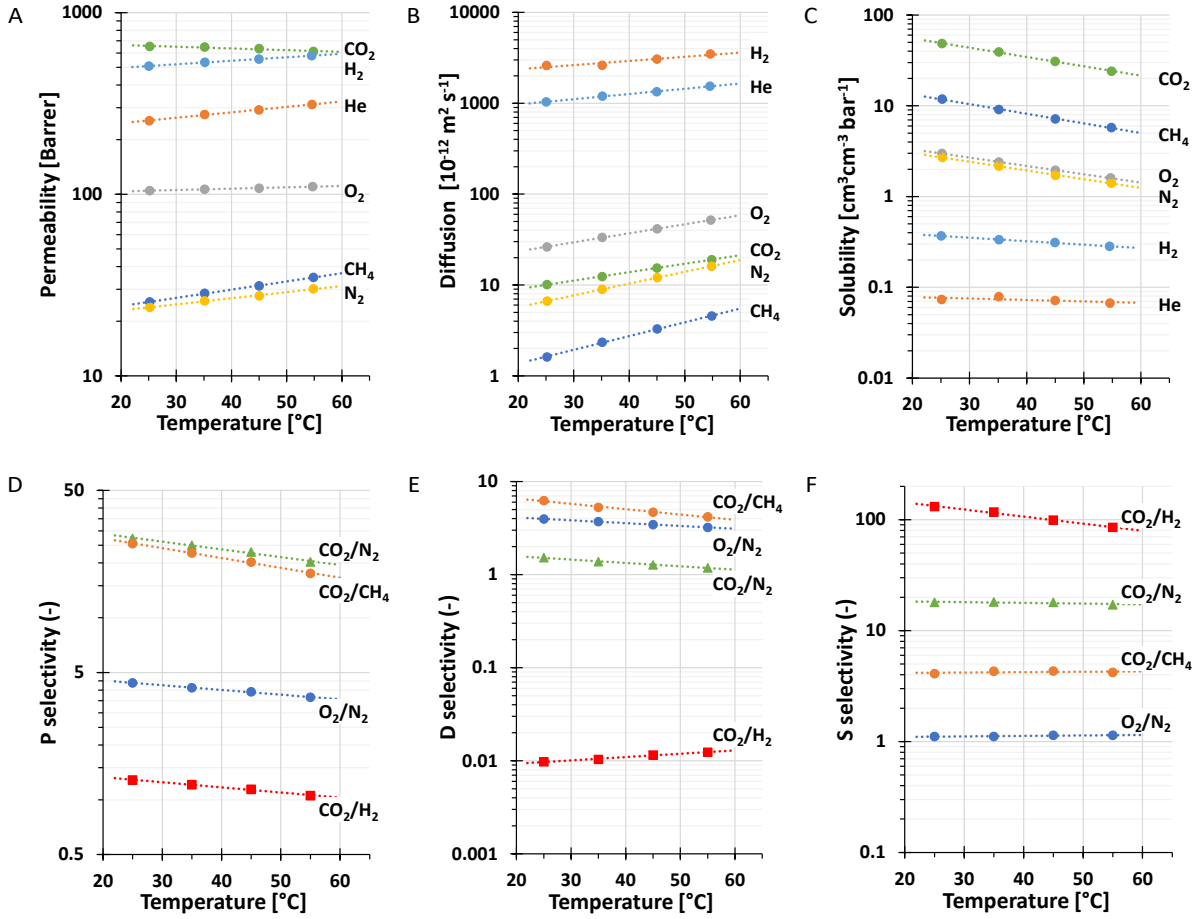

Figure 5. Temperature dependence of permeability (A), diffusivity (B) and solubility (C), and their corresponding selectivity for several gas pairs (C,D,E) in the PIM-Cardo-TOT 543 days aged films. The dotted lines represent an exponential fit and are plotted as a guide to the eye.

Table 3 Activation Energies for Permeation (E_p, Eq. 4) and Diffusion (E_d, Eq. 5); Heat of Sorption (H_s, Eq. 6), Diffusion Selectivity (D_i/D_{N2}) and Correlated Energetic and Entropic Selectivity with respect to N_2 at 25 °C in aged Cardo-PIM-TOT and PIM-TOT-SBF-5.

Property	Polymer	Gas					
		N_2	O_2	CO_2	CH_4	H_2	He
E_p [kcal/mol]	PIM-Cardo-TOT	1.51	0.33	-0.42	2.03	0.86	1.33
	PIM-TOT-SBF-5	0.74	-0.52	-1.49	1.23	0.06	0.77
H_s [kcal/mol]	PIM-Cardo-TOT	-4.30	-4.11	-4.58	-4.75	-1.70	-0.69
	PIM-TOT-SBF-5	-4.08	-3.78	-4.91	-4.69	-1.89	-0.42
E_d [kcal/mol]	PIM-Cardo-TOT	5.80	4.44	4.17	6.78	2.57	2.03
	PIM-TOT-SBF-5	4.82	3.25	3.42	5.92	1.95	1.19
Diffusion selectivity (i/N_2)	PIM-Cardo-TOT	-	3.95	1.52	0.24	156	391
	PIM-TOT-SBF-5	-	2.92	1.19	0.42	48.9	76.4
Energetic selectivity (i/N_2)	PIM-Cardo-TOT	-	10.0	15.9	0.19	237	588
	PIM-TOT-SBF-5	-	14.1	10.6	0.16	127	459
Entropic selectivity (i/N_2)	PIM-Cardo-TOT	-	0.44	0.10	1.15	1.33	1.94
	PIM-TOT-SBF-5	-	0.23	0.11	2.46	0.78	0.49

Interestingly, **PIM-Cardo-TOT** possesses a high entropic selectivity (>1) for H_2/N_2 and He/N_2, which would suggest that small local relaxations of the polymer chains allow rotational and/or vibrational modes of these small gas molecules in the activated region, which is unusual for PIMs but can be ascribed to the relative of ease of motion about the cardo centre, which deviates from the more rigid ladder-like structure associated with PIMs. In addition, local motions within the polymer chain may also be attributed to the conformational flexibility of the non-planar TOT unit.[44] The H_2/N_2 and He/N_2 energetic selectivities are very high for both the PIMs-TOT, since the opening of a motion-enabled-zone for the diffusion of H_2 and He requires a small chain displacement due to their small effective diameters. Their values, as well as those involving bulkier gases, are half-way between those of PIM-1 and PIM-BTrip/PIM-TMN-Trip.[39] **PIM-Cardo-TOT** shows higher energetic selectivities than **PIM-TOT-SBF-5**, due to its higher polymer chain cohesion. This is consistent with the lower N_2 adsorption and flatter isotherm obtained at 77 K for **PIM-Cardo-TOT** with respect to that of **PIM-TOT-SBF-5** (a), which can be attributed to smaller swelling of **PIM-Cardo-TOT** during the N_2 uptake, consistent with a relatively high polymer cohesion. In contrast, the *t-butyl* substituent on the spiro-centre in **PIM-TOT-SBF-5** disrupts its polymer cohesion, reducing the energetic selectivity, but increasing the overall gas diffusion.

Conclusions

The synthesis of a series of dibenzodioxin-based PIMs derived from different bis-catechol-containing monomers in combination with the 2,3,7,8-tetrafluoro-5,5',10,10'-tetra-oxidethianthrene monomer (**TOT**) was achieved via small modifications of previously reported synthetic paths. They exhibited high porosity, good thermal stability, and six of them also formed self-standing films from which gas permeability data could be measured. In general, all six **PIM-TOT** polymers showed encouraging performance for gas separation, with lower permeability but higher selectivity, as compared with archetypal PIM-1 and the corresponding PIMs derived from 2,3,5,6-tetrafluoroterephthalonitrile (TFTPN). Their permselectivity increases upon ageing, commonly attributed to an overall decrease in high free volume of PIMs and to a tightening of the bottlenecks between the free volume elements, which strongly increases the diffusion selectivity. The latter is mainly governed by the energetic selectivity, especially in polymers that can pack more efficiently due to the relatively larger degree of rotation and flexibility of the composing monomers. In contrast, the presence of more rigid structural units such as SBF, reduces the packing efficiency, which corresponds to a decrease of the activation energy of diffusion and, in turn, an increase in permeability. The highly chemically and thermally stable tetraoxidethianthrene unit can be considered a useful alternative component for preparing PIMs for applications in gas separation membranes, especially for use in acidic environments that could result in hydrolysis of nitrile. These PIM offer far superior permeability when compared with polysulfones reported in the literature.

Conflicts of interest.

The authors declare no conflict of interest

Acknowledgements

The research leading to these results has received funding from the EU FP7 Framework Program under grant agreement n° 608490, project M^4CO_2

References

1. N. B. McKeown and P. M. Budd, *Macromolecules*, 2010, **43**, 5163-5176.
2. H. J. Mackintosh, P. M. Budd and N. B. McKeown, *J. Mater. Chem.*, 2008, **18**, 573-578.
3. P. Budd, N. McKeown, B. Ghanem, K. Msayib, D. Fritsch, L. Starannikova, N. Belov, O. Sanfirova, Y. Yampolskii and V. Shantarovich, *J. Membr. Sci.*, 2008, **325**, 851-860.
4. N. B. McKeown, B. Gahnem, K. J. Msayib, P. M. Budd, C. E. Tattershall, K. Mahmood, S. Tan, D. Book, H. W. Langmi and A. Walton, *Angew. Chem. Int. Ed. Engl.*, 2006, **45**, 1804-1807.
5. B. S. Ghanem, M. Hashem, K. D. M. Harris, K. J. Msayib, M. Xu, P. M. Budd, N. Chaukura, D. Book, S. Tedds, A. Walton and N. B. McKeown, *Macromolecules*, 2010, **43**, 5287-5294.

6. T. Anokhina, A. Yushkin, P. Budd and A. Volkov, *Sep. Purif. Technol.*, 2015, **156**, 683-690.
7. H. Ye, C. Zhang, C. Huo, B. Zhao, Y. Zhou, Y. Wu and S. Shi, *Polymer Reviews*, 2020, 1-41.
8. E. Al-Hetlani, M. O. Amin, C. G. Bezzu and M. Carta, *R. Soc. Open Sci.*, 2020, **7**, 200741.
9. N. B. McKeown, P. M. Budd, K. J. Msayib, B. S. Ghanem, H. J. Kingston, C. E. Tattershall, S. Makhseed, K. J. Reynolds and D. Fritsch, *Chem. Eur. J.*, 2005, **11**, 2610-2620.
10. L. M. Robeson, *J. Membr. Sci.*, 1991, **62**, 165-185.
11. N. Du, G. P. Robertson, J. Song, I. Pinnau, S. Thomas and M. D. Guiver, *Macromolecules*, 2008, **41**, 9656-9662.
12. L. M. Robeson, *J. Membr. Sci.*, 2008, **320**, 390-400.
13. N. Du, G. P. Robertson, I. Pinnau and M. D. Guiver, *Macromolecules*, 2010, **43**, 8580-8587.
14. K. E. Hart, L. J. Abbott, N. B. McKeown and C. M. Colina, *Macromolecules*, 2013, **46**, 5371-5380.
15. D. Fritsch, G. Bengtson, M. Carta and N. B. McKeown, *Macromol. Chem. Phys.*, 2011, **212**, 1137-1146.
16. B. S. Ghanem, N. B. McKeown, P. M. Budd and D. Fritsch, *Macromolecules*, 2008, **41**, 1640-1646.
17. C. G. Bezzu, M. Carta, M.-C. Ferrari, J. C. Jansen, M. Monteleone, E. Esposito, A. Fuoco, K. Hart, T. P. Liyana-Arachchi, C. M. Colina and N. B. McKeown, *J. Mater. Chem. A*, 2018, **6**, 10507-10514.
18. T. Emmler, K. Heinrich, D. Fritsch, P. M. Budd, N. Chaukura, D. Ehlers, K. Rätzke and F. Faupel, *Macromolecules*, 2010, **43**, 6075-6084.
19. M. Carta, R. Malpass-Evans, M. Croad, Y. Rogan, J. C. Jansen, P. Bernardo, F. Bazzarelli and N. B. McKeown, *Science*, 2013, **339**, 303-307.
20. M. Carta, P. Bernardo, G. Clarizia, J. C. Jansen and N. B. McKeown, *Macromolecules*, 2014, **47**, 8320-8327.
21. I. Rose, C. G. Bezzu, M. Carta, B. Comesana-Gandara, E. Lasseuguette, M. C. Ferrari, P. Bernardo, G. Clarizia, A. Fuoco, J. C. Jansen, K. E. Hart, T. P. Liyana-Arachchi, C. M. Colina and N. B. McKeown, *Nat. Mater.*, 2017, **16**, 932-937.
22. B. Comesaña-Gándara, J. Chen, C. G. Bezzu, M. Carta, I. Rose, M.-C. Ferrari, E. Esposito, A. Fuoco, J. C. Jansen and N. B. McKeown, *Energy Environ. Sci.*, 2019, **12**, 2733-2740.
23. K. N. Fujii, Tomomasa;, *Jpn. Kokai Tokyo Koho*, 2007.
24. P. M. Budd, E. S. Elabas, B. S. Ghanem, S. Makhseed, N. B. McKeown, K. J. Msayib, C. E. Tattershall and D. Wang, *Adv. Mater.*, 2004, **16**, 456-459.
25. *The University of Manchester, UK . Pat.,* WO2005012397A2, 2005.
26. S. C. Fraga, M. Monteleone, M. Lanč, E. Esposito, A. Fuoco, L. Giorno, K. Pilnáček, K. Friess, M. Carta, N. B. McKeown, P. Izák, Z. Petrusová, J. G. Crespo, C. Brazinha and J. C. Jansen, *J. Membr. Sci.*, 2018, **561**, 39-58.
27. J. Crank, *The Mathematics of Diffusion. 2d Ed*, 1975.
28. J. B. Niederl and R. H. Nagel, *J. Am. Chem. Soc.*, 1940, **62**, 3070-3072.
29. M. Thommes and K. A. Cychosz, *Adsorption*, 2014, **20**, 233-250.
30. P. Bernardo, F. Bazzarelli, F. Tasselli, G. Clarizia, C. R. Mason, L. Maynard-Atem, P. M. Budd, M. Lanč, K. Pilnáček and O. Vopička, *Polymer*, 2017, **113**, 283-294.
31. R. Swaidan, B. Ghanem and I. Pinnau, *ACS Macro Lett.*, 2015, **4**, 947-951.
32. A. W. Thornton, B. D. Freeman and L. M. Robeson, https://membrane-australasia.org/msa-activities/polymer-gas-separation-membrane-database/, (accessed December 2020).
33. D. F. Sanders, Z. P. Smith, R. Guo, L. M. Robeson, J. E. McGrath, D. R. Paul and B. D. Freeman, *Polymer*, 2013, **54**, 4729-4761.
34. Z.-X. Low, P. M. Budd, N. B. McKeown and D. A. Patterson, *Chem. Rev.*, 2018, **118**, 5871-5911.
35. R. R. Tiwari, J. Jin, B. D. Freeman and D. R. Paul, *J. Membr. Sci.*, 2017, **537**, 362-371.
36. A. Fuoco, C. Rizzuto, E. Tocci, M. Monteleone, E. Esposito, P. M. Budd, M. Carta, B. Comesaña-Gándara, N. B. McKeown and J. C. Jansen, *J. Mater. Chem. A*, 2019, **7**, 20121-20126.
37. V. Teplyakov and P. Meares, *Gas Sep. Purif.*, 1990, **4**, 66-74.
38. T. Masuda, Y. Iguchi, B.-Z. Tang and T. Higashimura, *Polymer*, 1988, **29**, 2041-2049.
39. A. Fuoco, B. Comesaña-Gándara, M. Longo, E. Esposito, M. Monteleone, I. Rose, C. G. Bezzu, M. Carta, N. B. McKeown and J. C. Jansen, *ACS Appl. Mater. Interfaces*, 2018, **10**, 36475-36482.
40. P. Li, T. S. Chung and D. R. Paul, *J. Membr. Sci.*, 2014, **450**, 380-388.
41. W. J. Koros and C. Zhang, *Nat. Mater.*, 2017, **16**, 289-297.
42. A. Singh-Ghosal and W. J. Koros, *Ind. Eng. Chem. Res.*, 1999, **38**, 3647-3654.
43. C. M. Zimmerman and W. J. Koros, *Macromolecules*, 1999, **32**, 3341-3346.
44. D. Casarini, C. Coluccini, L. Lunazzi and A. Mazzanti, *The Journal of Organic Chemistry*, 2006, **71**, 6248-6250.